Diffusion Propagator Imaging with Model-Driven Regularization

Marco Reisert and Valerij G. Kiselev

Department of Radiology, Medical Physics
University Medical Center Freiburg, Freiburg, Germany
marco.reisert@uniklinik-freiburg.de

Abstract: The robust and accurate estimation of the ensemble average diffusion propagator (EAP), based on diffusion-sensitized magnetic resonance images, is an important preprocessing step for tractography algorithms or any other derived statistical analysis. In this work, we propose a new regularization strategy for EAP estimation that bridges the gap between model-based and model-free approaches. The idea is to use a Gaussian prior density which is especially designed for the diffusion signal in the human brain. Therefore, we propose to compute covariance statistics over a family of functions that are typical for human brain white matter. As the considered functions and the physically observed EAPs are usually smooth and local the Gauss-Laguerre basis system is used for realization. In various simulations and in-vivo experiments we show the effectiveness of the approach.

1 Introduction

Magnetic resonance imaging is able to non-invasively visualize the fibrous structure of the human brain white matter [Jon10]. Basically, one measures diffusion in many different directions (High Angular Resolution Diffusion Imaging - HARDI) in each voxel using diffusion-sensitized MRI. The aim is to obtain a set of values for each voxel, each associated with a certain direction, describing a probability index. This type of function is usually called a orientation distribution function (ODF). Usually one distinguishes between fiber ODFs and diffusion ODFs. A fiber ODF describes an index for the number of fibers passing a voxel in a particular direction. Diffusion ODFs give the probability for the displacement of water molecules. In this work we focus on the reliable estimation of the diffusion ODF. Accurate estimation of diffusion ODFs is important, particularly, for deterministic tractography algorithms [MCCvZ99, BPP$^+$00], where decisions during tracking are typically based on the local maxima of the ODF. But also for voxel wise statistics [SJ06] and diffusion based integrity measures [FLMS10] a reliable preprocessing of the data is a major prerequisite.

There are numerous methods for estimating the diffusion ODF: classical Q-ball imaging [Tuc04], probability density estimation [ALS09, TVWAF09, CRMGIM09,

erschienen im Tagungsband der INFORMATIK 2011
Lecture Notes in Informatics, Band P192
ISBN 978-3-88579-286-4

OSV+06, Bar09] and spatially regularized density estimation [RK11]. The underlying assumption in Q-ball imaging is that the measured signal and the ensemble average diffusion propagator (EAP) are connected via Fourier transformation (the narrow-pulse assumption for the Stejskal-Tanner sequence). The main problem is that the signal is usually measured on a single shell in q-space. Due to the 'global' nature of the Fourier transformation a direct transformation is not possible. Q-ball imaging in its early version [Tuc04] solved the problem via the so called Funk-Radon Transform. Basically, for each direction an average over the associated equator line is computed. This approach has the inherent problem of widening the resulting ODF due to an improper treatment of the solid angle. Extensions were introduced by several authors [ALS09, TVWAF09, CRMGIM09, OSV+06] where a mathematical sound investigation leads to well defined ODFs. The underlying assumptions of all these approaches is, more a less, an exponentially decaying signal in radial direction. This makes it possible to extrapolate the signal over the whole q-space to compute the Fourier transformation.

The idea presented in this work is more related to quite recent research [ATB09, OKS+09, DDB+10, CGJD10], which uses special types of basis functions to reconstruct and extrapolate the diffusion signal over the whole 3D space. But our starting point is different. We propose to use a problem-specific Gaussian prior density as prior distribution. Therefore, we compute covariance statistics over a family of model-functions that are typical for human white/gray matter and use the inverse of the resulting covariance operator as a regularizer during the estimation process. Indeed, this idea does not depend on the functional basis one is working with, but from a computational point of view, it is convenient to use a basis that is similar to the eigensystem of the covariance operator. Of course, the covariance operator must not depend on the absolute orientation, that is, it is an invariant tensor operator. It is well known that such an operator has a simple form in spherical harmonic (SH) representation. Thus, it is natural to use SHs in angular direction for representation. We additionally know that the EAP is usually smooth and local (in fact, an equivalent statement is: the diffusion signal is smooth and local). Hence, it is reasonable to use a basis that reflects this property. Therefore, we will use the Gauss-Laguerre (GL) basis that was already used in [OKS+09] (in a slightly different version in [ATB09, CGJD10]) for EAP imaging. A very convenient property of the GL-basis is that the Fourier transformation of a GL-function is again the same GL-function just with inverse scale.

The GL-basis is optimal for representing smooth and local functions. This is contrast to [DDB+10], where Laplace's equation is used to derive a proper set of basis functions, which only assumes smoothness (by Laplace's equation). Unfortunately, the smoothness and locality assumption causes a problem, it features an absolute scale (note that for a 'single' smoothness assumption this does not happen). Although the GL-basis is complete, artifacts occur if the GL expansion degree is too small and the scale of the GL-basis is too 'far' away from the measurement. This happens, for example, if the same scale is used for gray/white matter and cerebral spinal fluid. We will present a simple solution by extending the GL-basis by an

ISBN 978-3-88579-286-4

additional isotropic function matching the attenuation rates of water.

In the experiments we will show the advantages of our approach: (1) the resulting ODFs are linear in the signal, and hence, very efficient to compute and less susceptible to noise than other nonlinear approaches like [ALS09, TVWAF09, OSV$^+$06]. (2) for the proposed approach the measurements in q-space can be arbitrarily arranged. The treatment of single or multiple q-shell measurements is totally identical. Approaches that make use of 'exponential decay' assumption have to use multi-exponential models, which make them even more susceptible to noise. (3) as the complete 3D EAP is estimated, like in [DDB$^+$10] and [ATB09, CGJD10], several derived features and different types of diffusion ODFs can be computed. For example, the constant solid angle approach (CSA) of Aganj et al [ALS09], or the diffusion orientation transform (DOT, the EAP evaluated on a single shell) of Örzsalan [OSV$^+$06] are quite easy to compute.

2 Materials and Methods

Assume a diffusion weighted MR-signal E_i acquired for one or several b-values $b_i > 0$ and gradient directions $\mathbf{n}_i \in S_2$. As usual in q-ball imaging, we interpret the signal E_i as samples of a three-dimensional function, representing the EAP in q-space. The goal is to estimate and extrapolate E over the whole q-space from the relatively sparse measurements at locations[1] $\mathbf{q}_i = \mathbf{n}_i\sqrt{b_i/t}$, and transform the function by a Fourier transformation into real-space. To extrapolate E over the whole space, we have to include prior knowledge to complement the sparse measurement. We use two ways to formulate the prior knowledge: first, by a particular choice of basis functions, and second, by the type of regularizer which is used.

2.1 The Gauss-Laguerre Basis

We already stated in the beginning that we will use the so called Gauss-Laguerre basis. The idea is to look for a basis system which is simultaneously smooth and local. To measure smoothness and locality the following cost function is introduced:

$$R_{\mathrm{GL}}(E) = \frac{a^{-1}}{2}\int_{\mathbb{R}^3} |\nabla E(\mathbf{q})|^2 dq^3 + \frac{a}{2}\int_{\mathbb{R}^3} q^2 |E(\mathbf{q})|^2 dq^3$$

where the first term is a penalty on too rapid variations in q-space (the ∇ denotes the gradient operator) and the second one prefers functions that are located around

[1] Note that for consistency of the physical units we introduce here the diffusion time t. But, in the context of q-ball assumption the diffusion time t just rescales the q-space. Thus, we have to decide for a particular scale of the q-space to make quantitative statements. Thus, throughout the paper all quantitative statements refer to a diffusion time of $t = 1ms$.

ISBN 978-3-88579-286-4

the origin (local in q-space). The parameter $a > 0$ controls the balance between both demands. Note, that the formal appearance of this expression in q-space and real-space is identical. By looking in textbooks about quantum mechanics or theoretical chemistry [Fri06], more specifically the 3D harmonic oscillator, we can diagonalize the quadratic form representing R_{GL} with the orthonormal Gauss-Laguerre functions

$$\mathcal{G}^a_{n\ell m}(\mathbf{q}) := C_{n\ell a}\ L_n^{\ell+\frac{1}{2}}(aq^2) S_\ell^m(\sqrt{a}\mathbf{q}) e^{-aq^2/2}.$$

with normalization constant $C_{n\ell a} = \sqrt{\frac{n!(a/\pi)^{3/2}}{\Gamma(n+\ell+\frac{3}{2})}}$ with eigenvalues $N = 2n + \ell + \frac{3}{2}$. The Gauss-Laguerre functions $\mathcal{G}^a_{n\ell m}(\mathbf{q})$ share a remarkable property, which is very useful in our context. In fact, the GL-function is mapped by the Fourier transformation onto the same GL-function but with inverse scale. This property is particular useful for us, because the EAP and the MR-signal are connected by a Fourier transformation. That is, once we have found the expansion coefficients α of the GL expansion we have already the Fourier transform of the function for free.

2.2 Problem Specific Regularization

To get a representation of the signal in the subspace $W_N := \mathrm{span}(\{\mathcal{G}^a_{n\ell m} \mid 2n + \ell + \frac{3}{2} \leq N\})$ a usual way is to approximate the signal within W_N by minimizing an ordinary least square problem with a regularizer R:

$$I(\alpha) = \sum_i |\sum_{2n+\ell+3\leq N} \alpha_{n\ell m} \mathcal{G}^a_{n\ell m}(\mathbf{q}_i) - E_i|^2 + \lambda R(\alpha),$$

which is equivalent to the Maximum A-Posteriori (MAP) estimator with assuming a Gaussian data-likelihood and an exponential prior:

$$\alpha_{\mathrm{est}} = \underset{\alpha\in\mathbb{C}^d}{\mathrm{argmax}}\ p(\mathbf{E}|\alpha)p(\alpha) = \underset{\alpha\in\mathbb{C}^d}{\mathrm{argmax}}\, e^{-||\mathbf{G}\alpha-\mathbf{E}||^2} e^{-\lambda R(\alpha)}$$

If $R(\alpha) = \alpha^T \mathbf{R}\alpha$ is quadratic (that is, a Gaussian prior), the problem can be easily solved by inverting the normal equations $(\mathbf{G}^T\mathbf{G} + \lambda\mathbf{R})\alpha = \mathbf{G}^T\mathbf{E}$, where the entries of the matrix $\mathbf{G}$ are $G_{i,(n\ell m)} = \mathcal{G}^a_{n\ell m}(\mathbf{q}_i)$ and the elements of $\mathbf{E}$ are the MR-measurements E_i. The choice of the regularization matrix $\mathbf{R}$ is crucial to get reasonable results. If $R = R_{\mathrm{GL}}$, the matrix is diagonal with entries $(2n + \ell + \frac{3}{2})$ on its diagonal. We will see later that this choice already produces quite reasonable results, but there is actually another, more problem specific way to design R.

The idea is to consider a family of model functions, that is, functions that we expect as an outcome of our estimation procedure. Let $F = \{f_\gamma \mid \gamma \in \Gamma\}$ be a family of such functions with parameters γ taking values in a set Γ of possible values and further let $p(\gamma)$ be the probability that f_γ appears. For example, a nearby choice

ISBN 978-3-88579-286-4

would be

$$f_\gamma(\mathbf{q}) = \sum_{j=1}^{J} c_j \exp\left(-(D_j^{\text{fib}}(\mathbf{n}_j^T\mathbf{q})^2 + D_j^{\text{iso}}q^2)t\right), \tag{1}$$

where $\gamma = \{c_1, D_1^{\text{fib}}, D_1^{\text{iso}}, \mathbf{n}_j \ldots, c_J, D_J^{\text{fib}}, D_J^{\text{iso}}, \mathbf{n}_J\}$ are the parameters. The idea is to build a regularizer that favors functions belonging to this family. Therefore, we make second order statistics of the considered family by computing the corresponding covariance operator $\mathbf{K}$. If the inverse of the covariance operator is used as the quadratic regularizer $\mathbf{R} = \mathbf{K}^{-1}$, functions with the same covariance are preferred. It is implicitly assumed that the prior distribution is Gaussian with covariance $\mathbf{K}$.

In practice, the the GL-domain is well suited to represent the covariance operator $\mathbf{K}$ in matrix form. Let $(f^\gamma)_{n\ell m}$ be the GL-expansion coefficients of the function f_γ. For brevity we introduce a multi-index notation by writing a capital Greek letter, e.g. I, for the three indices n, ℓ, m. Then, the matrix elements of the covariance matrix $\mathbf{K}$ are $K_{I',I} = \sum_{\gamma\in\Gamma}\ p(\gamma)\ (f^\gamma)_{I'}\ \overline{(f^\gamma)_I}$. An important condition for the function family F is that it does not prefer any particular orientation, meaning that a rotated function $gf^\gamma = f^{\gamma'}$ has to appear with the same probability as the original f^γ within the family. Here $g \in SO(3)$ denotes are rotation of the function. Consequently, the sum over the family can be decomposed into an integral over the 3D rotation group $SO(3)$ and a sum over the residual quotient $\Gamma_0 = \Gamma/SO(3)$. Not surprisingly the GL-representation has very gentle properties with respect to $SO(3)$. In fact, one can show that the $SO(3)$-group integration let several terms vanish. For a derivation of this result see Appendix A. Thus, the covariance can be computed to

$$K_{I',I} = \delta_{\ell'\ell}\delta_{m'm}\frac{8\pi^2}{2\ell+1}\sum_{\gamma\in\Gamma_0} p(\gamma)\sum_{m=-\ell}^{\ell}(f^\gamma)_{n'\ell m}\overline{(f^\gamma)_{n\ell m}}. \tag{2}$$

Practically we compute the covariance matrix for a family of functions typical for the white matter in the human brain: we assume three compartments with equal contributions of $c_1 = c_2 = c_3 = 1/3$. The first two compartments are assumed to be of fibrous nature with $D_1^{\text{fib}} = D_2^{\text{fib}} =: D^{\text{fib}}$ and $D_1^{\text{iso}} = D_2^{\text{iso}} = 0.2D^{\text{fib}}$. The third is isotropic with $D_3^{\text{iso}} = 2\frac{\mu\text{m}^2}{\text{ms}}$ and $D_3^{\text{fib}} = 0$. To compute the covariance matrix we average over all possible angles between $\mathbf{n}_1$ and $\mathbf{n}_2$ of the two fiber compartments. Additionally we averaged also over D^{fib} for values between $0.8\frac{\mu\text{m}^2}{\text{ms}}$ and $3\frac{\mu\text{m}^2}{\text{ms}}$. In Figure 1 the covariance matrix is shown for a Gauss-Laguerre expansion up to $2n + \ell \leq 8$. For comparison the eigenvalues corresponding to the regularizer R_{GL} are plotted. One can notice that for $n = 0$, the diagonal entries of the covariance are particularly low, while for R_{GL} the penalty is more evenly distributed. Due to the low penalty for $n = 0$ the corresponding eigenfunction experience a low suppression during the fitting process. These eigenfunctions are so-called Gaussian-windowed solid-harmonics. The radial parts of the function are simply $q^\ell e^{-aq^2/2}$. One might suspect that only using the solid-harmonics instead of the whole Gauss-Laguerre expansion is advantageous. On the one hand, the solution of the corresponding problem is more regular, and, they are additionally

ISBN 978-3-88579-286-4

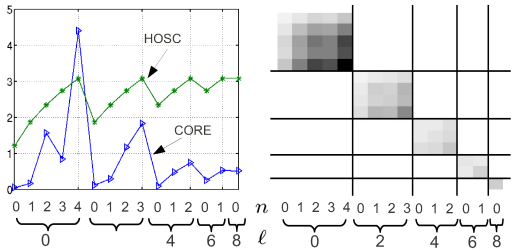

Figure 1: On the left the square-root of the diagonal entries of the covariance matrix in the GL-domain are plotted (COvariance REgularized, CORE). For comparison the diagonal entries of the regularizer R_{GL} are shown, which correspond to the eigenvalues of the Hamiltonian of the 3D quantum harmonic oscillator (Harmonic OSCillator, HOSC). The y-axis scaling for both plots is arbitrary. On the right the complete covariance matrix is depicted in gray-scale.

reflecting the type of functions we are interested in. In the following experiments we will consider these three different scenarios: a regularization by the above estimated covariance matrix (GL-CORE), regularization by R_{GL} based on the eigenvalues of the 3D harmonic oscillator (GL-HOSC), and just using the Gaussian-windowed solid-harmonics as a basis (GL-SOLID).

2.3 Determination of the Diffusion ODF

Usually people are interested in orientation distributions functions (ODF). To get an ODF similar to the one proposed by [ALS09] one can consider an integration along radial rays. One gets the probability that water-molecules are displaced into a certain direction regardless the amount of displacement. That is, we integrate the EAP P, which is the Fourier transformation of the estimated signal, along the radial coordinate with solid angle weight r^2:

$$P_{\mathrm{csa}}(\mathbf{n}) \quad = \quad \int_0^\infty P(\mathbf{r}) r^2 dr \sum_{n,\ell,m} \alpha_{n\ell m}\ \beta_{n\ell}^{\mathrm{csa}} Y_\ell^m(\mathbf{n}) \tag{3}$$

where the $\beta_{n\ell}^{\mathrm{csa}}$ are the integral $\beta_{n\ell}^{\mathrm{csa}} = C_{nla}\, \mathbf{i}^{2n+\ell} \int_0^\infty L_n^{\ell+\frac{1}{2}}(\frac{r^2}{a})(\frac{r}{\sqrt{a}})^\ell e^{-\frac{r^2}{2a}} r^2 dr$ which can be computed numerically or analytically.

A second way to obtain a meaningful ODF is to evaluate P on a certain shell with radius r_0, that is, one considers at the displacement probability for a fixed displacement length r_0. This approach was also investigated by Özarslan et al [OSV+06] and is called Diffusion Orientation Transform (DOT). In our framework the computation of the corresponding ODF is simple

$$P_{\mathrm{shell}}^{r_0}(\mathbf{n}) = P(r_0\mathbf{n}) = \sum_{n,\ell,m} \alpha_{n\ell m}\ \beta_{n\ell}^{\mathrm{shell}}(r_0) Y_\ell^m(\mathbf{n}) \tag{4}$$

with $\beta_{n\ell}^{\text{shell}}(r_0) = C_{nla}\mathbf{i}^{2n+\ell}L_n^{\ell+\frac{1}{2}}(\frac{r_0^2}{a})(\frac{r_0}{\sqrt{a}})^\ell e^{-\frac{r_0^2}{2a}}$ The larger the shell radius the 'sharper' the ODF will get.

We want to emphasize that for both former approaches, the one by Aganj et al [ALS09] and Özarslan et al [OSV+06], the resulting diffusion ODFs depend on the signal in a nonlinear way. Contrarily, in our method the whole treatment is carried out in a linear fashion. From this we can expect that the noise behaviour of the proposed approach should be much better, which we will see in experiments.

3 Experiments

It is instructive to start with a visual example on simulated data. The data was synthesized using equation (1) without any noise. Three compartments are assumed with equal contributions of $c_1 = c_2 = c_3 = 1/3$, two of fibrous nature with $D_1^{\text{fib}} = D_2^{\text{fib}} = 1.2\frac{\mu\text{m}^2}{\text{ms}}$ and $D_1^{\text{iso}} = D_2^{\text{iso}} = 0.2\frac{\mu\text{m}^2}{\text{ms}}$, and one isotropic compartment with $D_3^{\text{fib}} = 0$ and $D_3^{\text{iso}} = 2\frac{\mu\text{m}^2}{\text{ms}}$. The angle between the two fiber compartment was set to 75°. As a ground-truth the signal was synthesized on a dense Cartesian grid in q-space. The inverse Fourier transform of the ground-truth signal was computed analytically and also rendered onto a dense Cartesian grid. In Figure 2 (left) 2D slices through the crossing plane are shown. Based on the ground-truth signal, integrals along radial rays were computed analytically (CSA) and a EAP shell[2] at $r_0 = 3\mu$m was selected to compute the ODFs. The ground truth signal was sampled at a b-value of $q^2t = b = 2\frac{\text{ms}}{\mu\text{m}^2}$ for 128 gradient directions equally distributed over the sphere. These measurements E_i were used to apply our method (GL-CORE, GL-HOSC, GL-SOLID). The scale a of the GL-representation was set to $a = 3/4\mu$m and the regularization parameter $\lambda = 0.01$. Later we will discuss the choice of the two parameters in detail. The cutoff of the GL-expansion was set to $2n + \ell = 8$.

For comparison the common exponential decay assumption was applied to extrapolate the signal over the whole q-space. To render the exponentially extrapolated signal into 3D space, the signal was set to $E(q\mathbf{n}_i) = e^{q^2 t \log M_i/b}$ along the radial rays defined by $\mathbf{n}_i$. To get a smooth signal a trilinear, barycentric interpolation between neighboring radial rays was applied. The Fourier transform was computed by use of the FFT.

The lower two rows of Figure 2 (left) show the CSA integrals and the EAP at $r_0 = 3\mu$m (for a more realistic diffusion time of $t = 25$ms this corresponds to a radius of 15μm.) For the exponential models the algorithm of Aganj et al [ALS09] was used to compute the CSA integrals and the algorithm of Özarslan et al [OSV+06] for the diffusion propagator on the shell (basically the so called DOT). For Aganj's approach the spherical harmonic expansion was also cut off at $\ell = 8$ and the common Laplace-Beltrami regularization with $\lambda = 0.01$ was used.

Overall, the results of the different methods are similar. A closer look at the 2D

[2]The shell radius has to be understood in conjunction with a diffusion time of $t = 1$ms

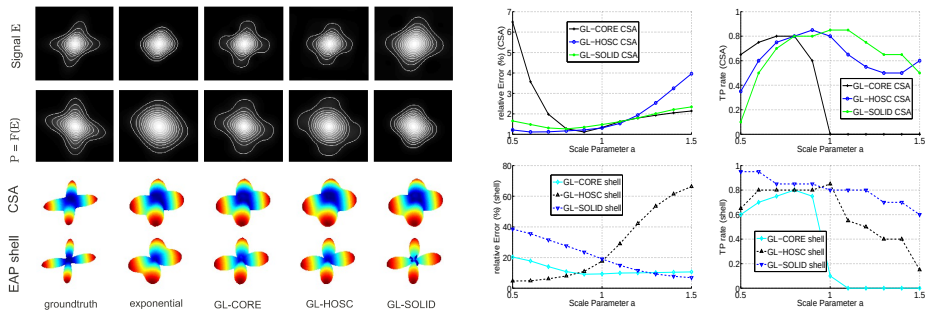

Figure 2: **Left:** Toy experiment on a simulated crossing of 75°. The signal was synthesized on a dense Cartesian grid. Slices through the crossing plane are shown in the top row, for $\mathbf{q}$ varying between $-4(\mu\text{m})^{-1}$ and $4(\mu\text{m})^{-1}$ and $\mathbf{r}$ varying between -4μm and 4μm. Our methods (GL-CORE/HOSC/SOLID) are compared with the usual 'exponential decay'-assumption. The lower two rows show the corresponding CSA integrals and the EAP at $r_0 = 3\mu$m as ODF glyphs. **Right:** To determine the optimal scale factor a of the GL-expansion we measured the performance of the approaches on a simulated crossing of 55° at a b-value of $2\frac{\text{ms}}{\mu\text{m}^2}$. The scale is given in μm in the above plots.

slices of the dense signal suggests that the 'exponential decay' assumption introduces a small 'blurr', this was already discussed in [OSV+06]. The blurr becomes particular visible for the EAP shell, the impact on the CSA integral is not strong. Comparing our methods, the GL-SOLID seems to produce the 'sharpest' results, but also produces some negative undershoots for the shell approach.

3.1 Parameters

Our approach contains basically three parameters, the scale a of the GL-expansion, the cutoff of the expansion $d = 2n+\ell$ and the regularization strength λ. We already explained that the scale controls the trade off between locality and smoothness. To find an optimal scale we simulated a 55° crossing at a b-value of $b = 2\frac{\text{ms}}{\mu\text{m}^2}$. The parameters of the simulation were the same as in the visual experiment from above. We added artificially Rician noise with a SNR of 50. We repeated the experiment 200 times to get stable results. In Figure 2 (right) we show the relative error[3] of the obtained CSA integrals and the shell approach by varying the scale between 0.5μm and 1.5μm. To measure the accuracy how well the underlying fiber directions are estimated we compute the rate of how often the local maxima of the estimated ODFs coincide with the true underlying direction. We say a fiber direction was detected if the ground truth directions are within a range of 10° from a local maximum of the estimated ODF. The number of all successfully resolved directions divided by the number of all directions is called the true positive

[3]By interpreting an estimated ODF as a vector $\mathbf{x}$ we defined the relative error to be error $= 100\% \cdot (1 - \frac{\mathbf{x}^T\mathbf{g}}{||\mathbf{x}||||\mathbf{g}||})$, where $\mathbf{g}$ is the ground-truth ODF.

rate (TP rate). A similar measure was already used in [RK11] to measure the performance of ODF estimations. Figure 2 (right) does not show a unique picture. It seems that GL-CORE works better with smaller scales with respect to the TP-rate, but with respect to the error small scales are only advantageous for the shell approach. Hence, it is not possible to make a decision which takes both into account. Throughout the paper we decided for a scale of 0.75μm. For λ similar problems occur. First, it depends on the noise which is expected, secondly we found that low values for λ promote good results for the CSA integrals, while the EAP shells are worse. The roles are exchanged for higher values of λ. We decided again for a compromise with a little bit of advantage for the shell approach. We decided for a $\lambda = 0.01$ throughout the whole paper. Fortunately, the decision for the cutoff d was more simple. We found that for values above 8 the performance was not getting any better, thus, we use $d = 8$. For the DOT approach [OSV$^+$06] and Aganj's [ALS09] CSA approach we also used a spherical harmonic cutoff band of 8, which seems to be enough.

3.2 Water Correction

Above we tailored the parameters of the GL-expansion to the white/gray matter of the human brain (in particular the scale parameter a and the diffusivity parameters). As the brain also contains cerebral spinal fluid (CSF) we can expect that our current approach will come into trouble in these regions. And this is indeed the case. The rather coarse GL-basis (with a rather small a) is not able to model the fast decay of the water signal and produces a kind of ringing artifact. In Figure 3 we applied the approach to in-vivo data at the transition area between white/gray matter and CSF. One can observe that the GL-fit produces several negative undershoots (in red) in the water regions. Correspondingly, the Fourier transform of the signal shows negative values around the origin $r = 0$. But, there is a simple way to solve the problem. The water signal can be easily modeled by a Gaussian with the correct width, thus, we use one additional basis function for modeling: a $\mathcal{G}^a_{00}$ (just a Gaussian) of scale $a = 2D^{\text{water}}t$. There is no need to use higher-order GL-functions, because the water signal is highly isotropic. No regularization was used for the additional function. In Figure 3 we show the results with 'water correction'. The negative values have disappeared almost completely. We also show the expansion coefficient of the fit for the additional Gaussian. It gives a clear indication for the water fraction within the signal.

3.3 Single Q-Shell Simulations

To measure the performance of our approach we did extensive simulations under various conditions. The b-value is varied, the SNR is varied and different tissue situations are compared. We compared our approach with three other approaches:

ISBN 978-3-88579-286-4

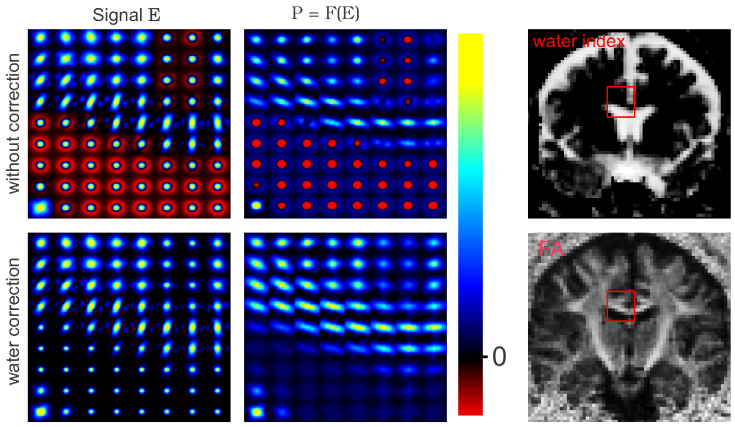

Figure 3: A coronal section of the human brain at a transition areas of white matter and CSF. The GL-fit (GL-CORE) of the signal and its Fourier transform (top left/middle) shows several negative undershoots in red. By using an additional Gaussian for modeling the water, the problem disappears (bottom left/middle) . The expansion coefficient of the additional Gaussian gives an indicator for water (top right, only positive values are displayed). A FA-map is displayed for orientation. The data was measured at a b-value of $b = 1\frac{\text{ms}}{\mu\text{m}^2}$ with $n = 61$ gradient directions.

two based on the 'exponential decay' assumption, namely [OSV+06] and [ALS09]. As a third method we applied the approach of Vega et al [TVWAF09] which is based on a slightly different approximation. The simulated signal were again computed on the basis of equation (1) with the parameters mentioned above, while we varied the crossing angle from 40° to 90°. Rician noise was added to the simulated signal by $E_{\text{noisy}} = |E + n_{\text{re}} + \mathbf{i}n_{\text{im}}|$ where n_{im} and n_{re} are Gaussian distributed with standard deviation 1/SNR. The number of gradient directions is 128. To measure the performance we computed, as described above, the relative errors of the estimated ODFs and the TP-rate of how well the local maximas of the ODF describe the underlying fiber directions. In the simulations we varied the b-values between $1\frac{\text{ms}}{\mu\text{m}^2}$ and $3\frac{\text{ms}}{\mu\text{m}^2}$, for the SNR we used 20 and 50. For the shell-based approach the shell radius was varied between 2μm and 5μm. We found that the relative error of the estimations do vary too much for different crossing angle. Thus, we averaged the error over all considered angles. The experiments were repeated 1000 times to obtain stable results. In Table 1 the errors are shown for the CSA integrals and the EAP-shells. For CSA the GL-CORE and GL-SOLID approaches perform best. The approach of Vega et al [TVWAF09] has big problems in a low SNR/b-value regime. For b-values lower than $3\frac{\text{ms}}{\mu\text{m}^2}$ there are high negative contributions, actually, inducing negative correlations with the ground-truth (In Table 1 a '-' indicates that the results had so many negative values such that the correlation with the ground-truth was negative) . For high SNRs the approach of Aganj et al [ALS09] shows comparable performance to GL. In Table 1 we show the same results with $b = 2\frac{\text{ms}}{\mu\text{m}^2}$

Table 1: Relative error rates

CSA

Parameter		Gauss Laguerre				
b-val	SNR	CORE	HOSC	SOLID	Aganj	Vega
1	10	7.7	4.0	**3.5**	8.8	-
	20	**3.0**	3.1	3.1	3.6	-
	50	**1.5**	2.9	3.0	2.3	-
2	10	3.5	3.1	**3.0**	6.4	-
	20	**1.6**	2.0	2.0	2.5	-
	50	**1.1**	1.6	1.7	1.2	-
3	10	**3.4**	4.4	4.0	6.7	49.1
	20	**1.4**	2.5	2.3	2.5	14.6
	50	**0.8**	1.8	1.7	1.3	8.3

EAP-shell

Parameter			Gauss Laguerre			
b-val	SNR	r_0	CORE	HOSC	SOLID	DOT
2	10	2	4.5	7.8	**3.9**	5.6
		3	**12.8**	13.6	27.1	16.9
		4	**15.5**	17.1	63.0	63.8
		5	**16.5**	17.2	85.1	90.2
	20	2	2.5	6.7	**1.6**	4.8
		3	**6.5**	6.9	16.4	7.6
		4	10.0	**9.4**	49.1	41.2
		5	11.8	**10.0**	76.4	82.6
	50	2	2.0	6.5	**1.0**	4.7
		3	**4.6**	5.0	12.3	5.9
		4	8.3	**7.2**	41.0	27.9
		5	10.4	**7.9**	67.9	71.9

for the shell-based approaches with shell radii $r_0 = 2, \ldots, 5\mu$m and compare GL to the DOT approach of Özarslan et al [OSV+06]. Again the GL performs better than the approach based on the 'exponential-decay' assumption. For small shell radii DOT is comparable to GL, but for larger radii DOT has severe problems. In Figure 4(left) all methods are evaluated with respect to the TP-rate at a SNR of 20. Again the crossing angle is varied between 40° and 90°. Considering the CSA integrals, the approach of Aganj and Vega is superior for high b-values. For lower b-values the GL approaches show better performance. Comparing the shell-based methods the 'exponential decay' assumption leads overall to worse results than the proposed methods. The differences become evident for low b-values where the approach of Özarslan [OSV+06] (DOT) performs very poor. One can also see that our approach can cope much better with larger shell radii. Another observation is that GL-SOLID can actually benefit from larger radii, while the performance of GL-CORE and GL-HOSC is similar or partially worsen for a radius of $r_0 = 5\mu$m. It is also astonishing that DOT is performing so poor for larger radii. To understand this effect consider Figure 4(right). The same signal as in the above experiments was simulated but without any noise at a b-value of $3\frac{\text{ms}}{\mu\text{m}^2}$. The diffusion propagator shell at $r_0 = 5\mu$m is visualized for different crossing angles. The GL-SOLID approach is compared to the DOT. Obviously, the DOT approach systematically overestimates the crossing angle. On the other hand, the local maximum of the GL-SOLID approach seems to be an unbiased estimator of the true underlying fiber direction.

3.4 In-Vivo Experiments

As quantitative evaluation of in-vivo data is difficult we want to restrict ourselves to some simple qualitative comparisons. In particular, we want to look at a scenario

which is clinical relevant[4], that is, we consider the low b-value regime at $b = 1\frac{\text{ms}}{\mu\text{m}^2}$ with a modest number of gradient directions (n=61). In Figure 5 the proposed approach (GL-CORE) is compared with the approach of Aganj et al [ALS09] for CSA integral computation and with the DOT by Özarslan et al [OSV$^+$06]. A coronal section of a healthy volunteer is shown. The parameters were all chosen the same as in the simulations. The regularization strength for our and Aganj's approach was set to 0.01 and the SH-cutoff to $d = 8$. Overall, our approach seems to produce the 'sharpest' results. As an example, look at the green rectangles in Figure 5. The crossing voxels are much more 'precise' with our approach. It was already reported by Özarslan [OSV$^+$06] that the 'exponential decay' assumption introduces a kind of blurring. On the other hand, one may argue that the difference is due to different regularization behavior or SH-expansions cutoffs. But, this is not the case. We also tried to lower the regularization strength for Aganj's approach, which led to a noise amplification but not a sharpening of the crossing. One can also look at the red rectangle, which contains two rather noisy voxels at the transition area of white matter and CSF. For Aganj's and Özarslan's approach they appear to be rather spikey, whereas our approach shows them more smooth. Additionally to the ODFs, we also show 2D slices of the complete signal (and its Fourier transform) in Figure 5 on the right.

4 Discussion and Conclusion

This work has proposed a novel framework for estimating the EAP by model-driven regularization. It can be used to estimate and extrapolate the EAP in a simple and effective way. It has been shown that the approach is more robust against noise than the usual 'exponential-decay' assumption. Which is mostly due to the linear nature of the GL-fit in comparison to the nonlinearities used in the other methods. That is, our framework is especially suited to work well in a low b-value and low SNR regime. It was also shown that the 'exponential-decay' assumption leads to systematic errors with respect to underlying fiber directions: for low angles the DOT overestimates the crossing angle. The comparison of the three GL-based methods has shown that GL-CORE produces the best results, while GL-SOLID is also competitive. Note, the simplicity of the GL-SOLID model: the complexity is just the same as in any other SH-based model, but the model is interpreted differently. It seems that Gaussian-windowed solid harmonics are special in the context of EAP modeling. Probably due to the fact that anisotropic diffusion comes along with an increased diffusivity, which is incorporated by the Gaussian-windowed solid harmonics. The higher the SH degree ℓ, the higher is the contribution for larger radii reflecting larger displacements.

[4]The in vivo diffusion measurements were acquired on a Siemens 3T TIM Trio using an SE EPI sequence, with a TE of 95 ms and a TR of 8.5 s. The whole brain was covered with contiguous 2 mm slices in an in-plane resolution of 2×2 mm^2. The diffusion encoding was performed in 61 directions with an effective b-value of $1\frac{\text{ms}}{\mu\text{m}^2}$.

ISBN 978-3-88579-286-4

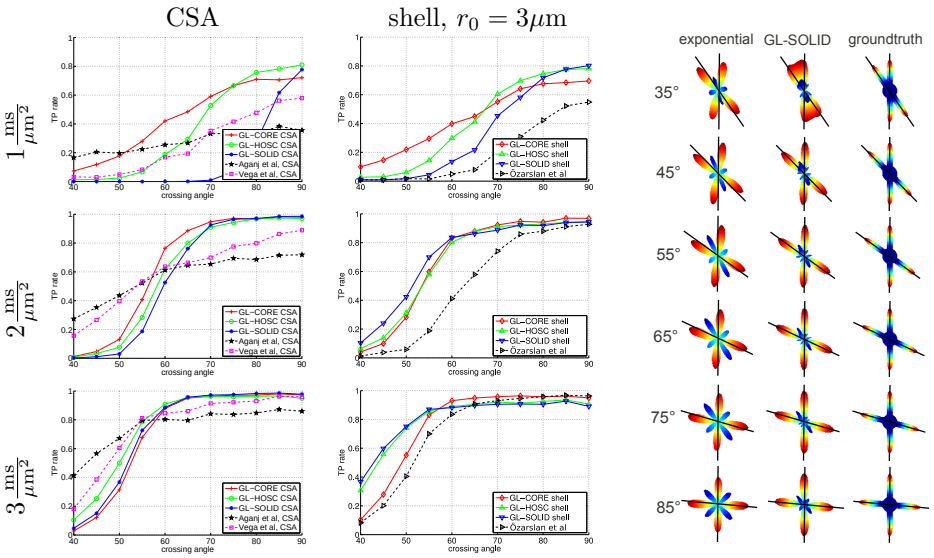

Figure 4: **Left:** TP-rates of simulations for different b-values at a SNR of 20. The TP-rate counts the number ODF local maxima that are within a range of 10° to the true fiber direction. **Right**: Comparison of GL-SOLID and the exponential approach (DOT) for a noise free simulation at a b-value of $3\frac{\text{ms}}{\mu\text{m}^2}$ and a r-shell of $r_0 = 5\mu$m. The true fiber directions are depicted by black sticks.

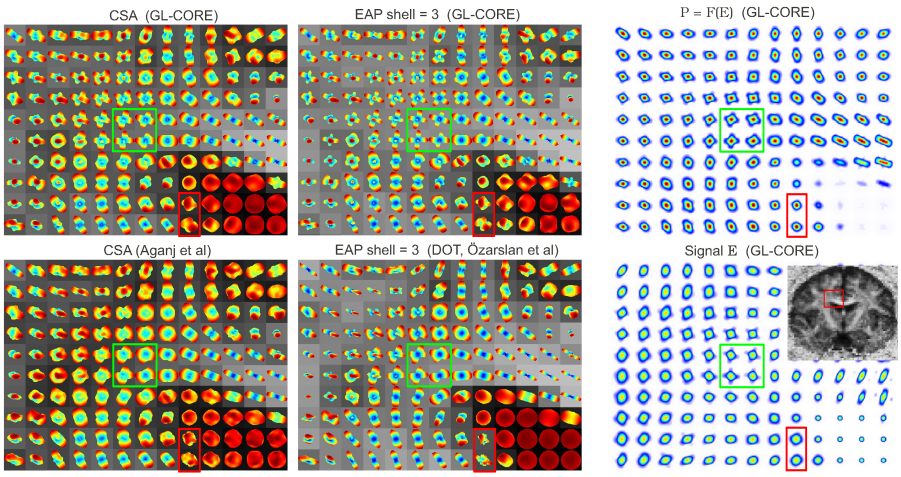

Figure 5: Qualititative comparison of GL-CORE with CSA [ALS09] and the DOT [OSV+06] (at a shell of $r_0 = 3\mu$m and $t = 1$ms) for a measurement with $b = 1\frac{\text{ms}}{\mu\text{m}^2}$ and $n = 61$ gradient directions. On the right the complete sliced EAP is shown.

In the experiments we focused on the single q-shell scenario. Comparisons with more recent multi-shell approaches like [DDB+10] are subject to future work. In particular, the comparison of the 'smoothness' assumption by [DDB+10] with our model-driven approach seems to be interesting. Another important point for future work involves the more reliable estimation of the covariance operator based on real measurements. But this will involve a very dense measurement of q-space.

Acknoledgements

The work of M. Reisert was supported by Deutsche Forschungsgemeinschaft (DFG), grant KI 1089/3-1. Thanks to I. Mader for providing the data.

Appendix

4.1 Group Integration of Covariance Matrix

A rotation $g \in SO(3)$ of a function f in GL-domain is accomplished by the socalled Wigner D-matrix $D^{\ell}_{mn}(g)$ (see e.g. [RH08]), i.e. if $(f)_{n\ell m}$ are the GL-coefficients of a function f, then the GL-representation of the rotated function gf looks like $(gf)_{n\ell m} = \sum_{k=-\ell}^{\ell} D^{\ell}_{mk}(g)\ (f)_{n\ell k}$ The Wigner D-matrix fulfills the following orthogonality relation $\int\limits_{SO(3)} D^{\ell'}_{m'k'}(g)\ \overline{D^{\ell}_{mk}(g)}\ dg = \delta_{\ell'\ell}\delta_{m'm}\delta_{k'k}\frac{8\pi^2}{2\ell+1}$ Inserting this into the integral

$$\int\limits_{SO(3)} (gf)_{n'\ell'm'}\ \overline{(gf)_{n\ell m}}\ dg = \delta_{\ell'\ell}\delta_{m'm}\frac{8\pi^2}{2\ell+1}\sum_{m=-\ell}^{\ell}(f)_{n'\ell m}\overline{(f)_{n\ell m}}.$$

gives the desired result.

References

[ALS09] I. Aganj, C. Lenglet, and G. Sapiro. ODF reconstruction in Q-ball imaging with solid angle consideration. In *Proceedings of IEEE Int. Symposium on Biomedical Imaging*, 2009.

[ATB09] Haz-Edine Assemlal, David Tschumperle, and Luc Brun. Evaluation of q-Space Sampling Strategies for the Diffusion Magnetic Resonance Imaging. In *Medical Image Computing and Computer-Assisted Intervention - MICCAI*, volume 5762, pages 406–414. Lecture Notes in Computer Science, Springer, 2009.

[Bar09] A. Barnett. Theory of Q-ball imaging redux: Implications for fiber tracking. *Magnetic Resonance in Medicine*, 62:910–923, 2009.

[BPP+00] P. J. Basser, S. Pajevic, C. Pierpaoli, J. Duda, and A. Aldroubi. In vivo fiber tractography using DT-MRI data. *Magn Reson Med*, 44(4):625–32, 2000. 20481737 0740-3194 Journal Article.

[CGJD10] Jian Cheng, Aurobrata Ghosh, Tianzi Jiang, and Rachid Deriche. Model-free and Analytical EAP Reconstruction via Spherical Polar Fourier Diffusion MRI. In *Medical Image Computing and Computer-Assisted Intervention - MICCAI*, 2010.

[CRMGIM09] E. J Canales-Rodriguez, L Melie-Garcia, and Y Iturria-Medina. Mathematical description of q-space in spherical coordinates: Exact q-ball imaging. *Magnetic Resonance in Medicine*, 61:1350–1367, 2009.

[DDB+10] Maxime Descoteaux, Rachid Deriche, Denis Le Bihan, Jean-FranÃ§ois Mangin, and Cyril Poupon. Multiple q-shell diffusion propagator imaging. *Medical Image Analysis, (in press)*, 2010.

[FLMS10] K.H. Fritzsche, F.B. Laun, H.P. Meinzer, and B. Stieltjes. Opportunities and pitfalls in the quantification of fiber integrity: What can we gain from Q-ball imaging? *Neuroimage*, 51:242–51, May 2010.

[Fri06] Harald Friedrich. *Theoretical atomic physics*. Birkhauser, 2006.

[Jon10] Derek K Jones, editor. *Diffusion MRI: Theory, Methods and Applications*. Oxford University Press, 2010.

[MCCvZ99] S. Mori, B. J. Crain, V. P. Chacko, and P. C. van Zijl. Three-dimensional tracking of axonal projections in the brain by magnetic resonance imaging. *Ann Neurol*, 45(2):265–9, 1999. 99142739 0364-5134 Journal Article.

[OKS+09] E. Ozarslan, C.G. Koay, T. Shepherd, S. Blackband, and P.J. Basser. Simple harmonic oscillator based reconstruction and estimation for three-dimensional q-space mri. In *International Society for Magnetic Resonance in Medicine (ISMRM)*, page 1396, 2009.

[OSV+06] Evren Oezarslan, Timothy M. Shepherd, Baba C. Vemuria, Stephen J. Blackband, and Thomas H. Marecid. Resolution of complex tissue microarchitecture using the diffusion orientation transform (DOT). *NeuroImage*, 31:1086–1103, 2006.

[RH08] M. Reisert and H.Burkhardt. Tensorial Harmonics for Efficient Tensor Voting in 3D. In *Proceedings of the CVPR'08*. IEEE Computer Society, 2008.

[RK11] M. Reisert and V. Kiselev. Fiber Continuity: An Anisotropic Prior for ODF Estimation. *IEEE Trans Med Imaging, (Epub avail.)*, 2011.

[SJ06] S. Smith and M. Jenkinson. Tract-based spatial statistics: Voxelwise analysis of multi-subject diffusion data. *NeuroImage*, 31(4):1487–1505, 2006.

[Tuc04] D. S. Tuch. Q-Ball imaging. *Magn. Reson. Med.*, 52(6):1358–1372, 2004. English 0740-3194.

[TVWAF09] Antonio Tristan-Vega, C.-F. Westin, and Santiago Aja-Fernandez. Estimation of fiber Orientation Probability Density Functions in High Angular Resolution Diffusion Imaging. *NeuroImage*, 47(2):638–650, 2009.

ISBN 978-3-88579-286-4

Diffusion Propagator Imaging by Model-driven Regularization

M. Reisert and V.G. Kiselev
Medical Physics, University Medical Center Freiburg, Freiburg, Baden Württemberg, Germany,
UNIVERSITY FREIBURG HOSPITAL

Introduction: Diffusion-weighted magnetic resonance imaging is able to non-invasively visualize the fibrous structure of the human brain white matter [1,2]. The robust and accurate estimation of the ensemble average diffusion propagator (EAP), based on diffusion-sensitized magnetic resonance images, is an important preprocessing step for tractography algorithms or any other derived statistical analysis ([3,4,5]). In this work, we propose a new regularization strategy for EAP estimation that bridges the gap between model-based and model-free approaches. The idea is to use a Gaussian prior density which is especially designed for the diffusion signal in the human brain. Therefore, we propose to compute covariance statistics over a family of functions that are typical for human brain white matter. As the considered functions and the physically observed EAPs are usually smooth and local the Gauss-Laguerre basis system [6] is used for realization. With this methodology it is possible to estimate the whole 3D EAP from a single q-shell measurement. In comparison to usual extrapolation strategies our approach is linear in the measured signal which makes it more robust to noise and partial volume effects. We will show this in synthetic and in-vivo experiments.

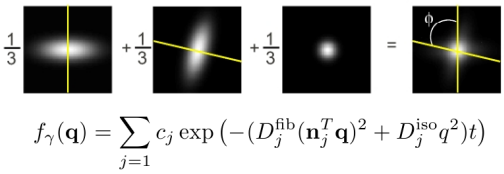

$$f_\gamma(\mathbf{q}) = \sum_{j=1} c_j \exp\left(-(D_j^{\mathrm{fib}}(\mathbf{n}_j^T\mathbf{q})^2 + D_j^{\mathrm{iso}}q^2)t\right)$$

Figure 1: The covariance matrix is estimated from an ensemble of synthetically created model functions that should cover the statistics of the signal of human brain white matter.

Methods: The usual assumption in EAP imaging is that the measured signal and the EAP are connected via a Fourier transform (FT).To infer the EAP P one has to apply the inverse FT, which is not possible directly, because the signal S is usually measured on a single q-shell (in a clinical environment). To solve the problem we follow a Bayesian approach. We search for most probable signal S (on the whole 3D q-space) given the measurement on a single q-shell, while assuming a certain Gaussian prior distribution. The Gaussian prior (its corresponding covariance matrix K) is estimated from synthetic data using common exponential model functions (see Figure 1). It is not feasible to work with the solution space in ordinary coordinate representation (it is consisting of 3D functions, hence, the covariance K would be a 6D array). Thus, the signal is represented by Gauss-Laguerre (GL) functions [6], which are a orthogonal functional basis and have very gentle properties with respect to the FT: the FT of a GL basis function is again the same GL function, but with inverse scale and multiplied by a phase factor. So, the computation of the FT, which is the final goal, comes for free. Once the full 3D EAP is estimated, derived features like Orientation Distribution Functions (ODF) based on the CSA integral [4] or the DOT [5] can be computed.

$$S(b,\mathbf{n}) = S(\mathbf{q}) = \int P(\mathbf{x}_1,\mathbf{x}_2,t)e^{\mathbf{i}\mathbf{q}\cdot(\mathbf{x}_1-\mathbf{x}_2)}d\mathbf{x}_1 d\mathbf{x}_2$$

$$\begin{aligned} p(\mathbf{S}|\mathbf{S}_{\mathrm{meas}}) &= p(\mathbf{S}_{\mathrm{meas}}|\mathbf{S})p(\mathbf{S}) \\ &= e^{-||\mathbf{S}-\mathbf{S}_{\mathrm{meas}}||^2}e^{-\lambda\mathbf{S}^T\mathbf{K}^{-1}\mathbf{S}} \end{aligned}$$

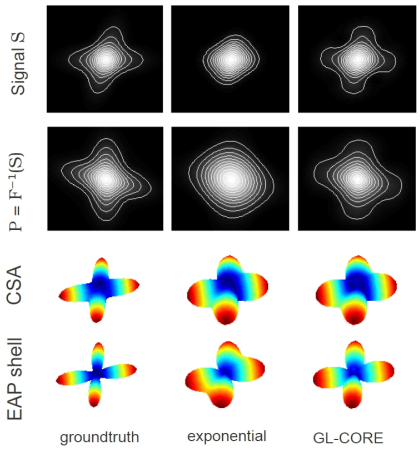

Figure 2: Comparison of the synthetically created ground truth signal S with the exponentially extrapolated signal and our approach (GL-CORE). Based on the FT of the extrapolated signal ($\mathrm{P}=\mathrm{F}(\mathrm{E})$) the constant solid angle (CSA) integral ODF is derived and a shell of the EAP is computed and shown as an ODF.

Results: Experiments were performed on simulations and in-vivo measurements. In comparison to CSA [4] and DOT [5] our approach shows a significant improvement with respect to reconstruction error and detection performance of the underlying fiber directions. In Figure 2 a visual example is shown: a signal was simulated over the whole q-space and sampled at b-value of 2000 s/mm² to simulate the measurement. We compare an exponential extrapolation ([4],[5]) with our approach (GL-CORE). Quantitatively, a crossing simulations with a b-value of 2000 s/mm² with a SNR of 20 gives for our approach a relative error of 2.5% to the ground truth, while the DOT approach shows an error of 4.8% (average over all crossing angles). Furthermore, the angle of crossing fibers can be detected earlier by our method in comparison to the CSA and DOT approach. The in-vivo measurements in Figure 3 were acquired with a isotropic 2mm resolution, 61 gradient directions with a b-value of 1000 s/mm². An example of crossing area near the corpus callosum is shown based on our approach and CSA [4].

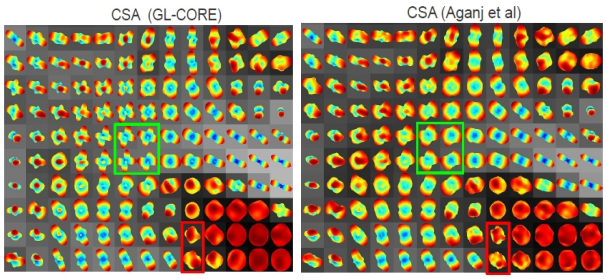

Figure 3: Comparison of in-vivo data. Our approach shows more well defined crossings (green), while reducing the noise (red), in particular in areas with partial volume effects.

Discussion: There are several advantages of the new approach. The resulting ODFs and features are linear in the signal, and hence, very efficient to compute and less susceptible to noise than other nonlinear approaches like [3,4,5]. Furthermore, for the proposed approach the measurements in q-space can be arbitrarily arranged. The treatment of single of multiple q-shell measurements are totally identical. Approaches that make use of the 'exponential decay' assumption ([3,4,5]) have to use multi-exponential models, which make them even more susceptible to noise. As the complete 3D EAP is estimated several derived features and different types of diffusion ODFs can be computed.

References: [1] Tuch et al, Q-ball imaging, MRM vol.52, no 6, pp 1358, 2004, [2] Jones, Diffusion MRI, Theory, Methods and Applications. Oxford University Press, 2010 [3] Vega et al., Estimation of fiber orientation probability density functions in high angular resolution diusion imaging," NeuroImage, vol. 47, no. 2 pp. 638, 2009, [4] Aganj et al, ODF reconstruction in q-ball imaging with solid angle consideration, ISBI 2009, [5] Özarslan et al, Resolution of complex tissue microarchitecture using the diffusion orientation transform (DOT), NeuroImage, vol. 31, pp. 1086, [6] Özarslan et al, Simple harmonic oscillator based reconstruction and estimation for three-dimensional q-space MRI, ISMRM 2009

Acknowledgements: The work of M. Reisert was supported by DFG, grant KI 1089/3-1.

Diffusion Propagator Imaging with Model-Driven Regularization

Marco Reisert and Valerij G. Kiselev

Department of Radiology, Medical Physics
University Medical Center Freiburg, Freiburg, Germany
marco.reisert@uniklinik-freiburg.de

Abstract: The robust and accurate estimation of the ensemble average diffusion propagator (EAP), based on diffusion-sensitized magnetic resonance images, is an important preprocessing step for tractography algorithms or any other derived statistical analysis. In this work, we propose a new regularization strategy for EAP estimation that bridges the gap between model-based and model-free approaches. The idea is to use a Gaussian prior density which is especially designed for the diffusion signal in the human brain. Therefore, we propose to compute covariance statistics over a family of functions that are typical for human brain white matter. As the considered functions and the physically observed EAPs are usually smooth and local the Gauss-Laguerre basis system is used for realization. In various simulations and in-vivo experiments we show the effectiveness of the approach.

The usual assumption in EAP imaging is that the measured signal and the EAP are connected via a Fourier transform (FT). To infer the EAP one has to apply the inverse FT, which is not possible directly, because the signal is usually measured on a single q-shell (in a clinical environment). To solve the problem we follow a Bayesian approach. We search for most the probable signal (on the whole 3D q-space) given the measurement on a single q-shell, while assuming a certain Gaussian prior distribution. The Gaussian prior (its corresponding covariance matrix) is estimated from synthetic data using common exponential model functions. Experiments were performed on simulations and in-vivo measurements. In comparison to others our approach shows a significant improvement with respect to reconstruction error and detection performance of the underlying fiber directions. Quantitatively, a crossing simulations with a b-value of $2000 s/mm^2$ with a SNR of 20 gives for our approach a relative error of 2.5% to the ground truth, while the DOT approach shows an error of 4.8% (average over all crossing angles). Furthermore, the angle of crossing fibers can be detected earlier. There are several advantages of the new approach. The resulting ODFs and features are linear in the signal, and hence, very efficient to compute and less susceptible to noise than other nonlinear approaches. Furthermore, for the proposed approach the measurements in q-space can be arbitrarily arranged. The treatement of single or multiple q-shell measurements are totally identical. As the complete 3D EAP is estimated several derived features and different types of diffusion ODFs can be computed.

erschienen im Tagungsband der INFORMATIK 2011
Lecture Notes in Informatics, Band P192
ISBN 978-3-88579-286-4